Provided for non-commercial research and education use.
Not for reproduction, distribution or commercial use.

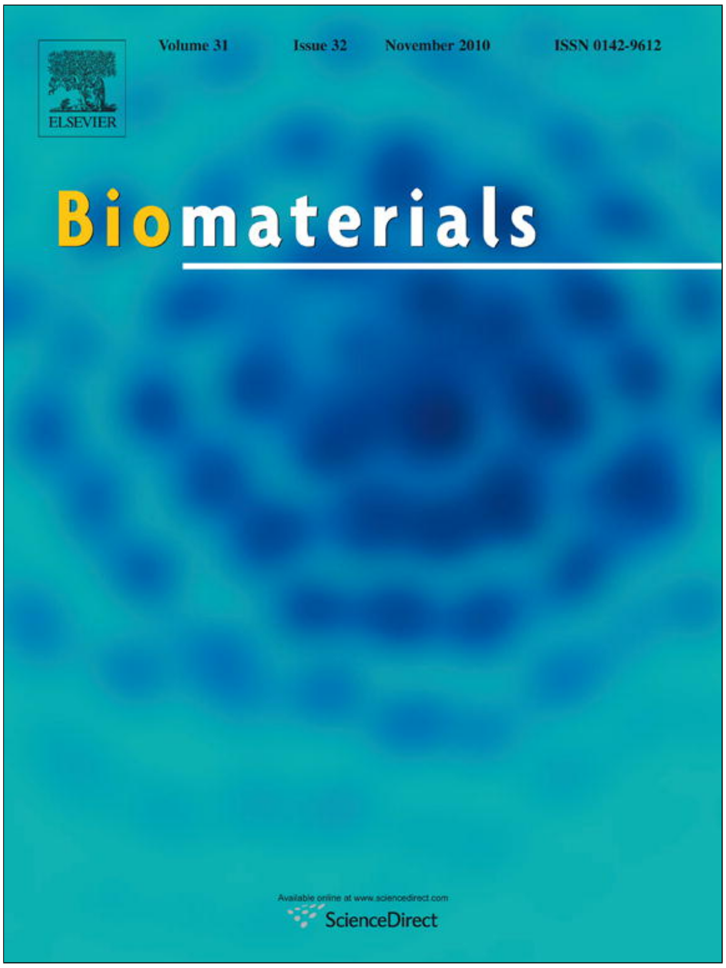
Volume 31
Issue 32
November 2010
ISSN 0142-9612
ELSEVIER
Biomaterials
Available online at www.sciencedirect.com
ScienceDirect

This article appeared in a journal published by Elsevier. The attached copy is furnished to the author for internal non-commercial research and education use, including for instruction at the authors institution and sharing with colleagues.

Other uses, including reproduction and distribution, or selling or licensing copies, or posting to personal, institutional or third party websites are prohibited.

In most cases authors are permitted to post their version of the article (e.g. in Word or Tex form) to their personal website or institutional repository. Authors requiring further information regarding Elsevier's archiving and manuscript policies are encouraged to visit:

http://www.elsevier.com/copyright

Biomaterials 31 (2010) 8228–8234

Contents lists available at ScienceDirect

Biomaterials

journal homepage: www.elsevier.com/locate/biomaterials

Patterning network structure to spatially control cellular remodeling and stem cell fate within 3-dimensional hydrogels

Sudhir Khetan, Jason A. Burdick*

Department of Bioengineering, University of Pennsylvania, 210 S 33rd Street, Philadelphia, PA 19104, USA

ARTICLE INFO

Article history:
Received 11 June 2010
Accepted 6 July 2010
Available online 31 July 2010

Keywords:
Hydrogels
Stem cells
Patterning
Remodeling
Hyaluronic acid

ABSTRACT

The spatially directed 3-dimensional (3D) remodeling of synthetic materials may be useful to regionally control cell behavior. In this work, we developed a process to synthesize hyaluronic acid hydrogels using multiple modes of crosslinking applied sequentially; a primary addition reaction to introduce protease degradable peptide crosslinks, then a UV light-induced secondary radical reaction (enabling spatial control) to introduce non-degradable kinetic chains. These differential network structures either permitted (primary crosslinking only, "−UV") or inhibited (sequential crosslinking, "+UV") cellular remodeling. This behavior was validated by controlling the outgrowth from chick aortic arches or the spreading of encapsulated mesenchymal stem cells (MSCs), where only −UV regions permitted arch outgrowth and MSC spreading. Additionally, network structures dictated adipogenic/osteogenic MSC fate decisions, with spatial control, by controlling encapsulated MSC spreading. This manipulation of microenvironmental cues may be valuable for advanced tissue engineering applications requiring the spatial control of cells in 3D.

© 2010 Elsevier Ltd. All rights reserved.

1. Introduction

The 3-dimensional (3D) interactions of cells and the extracellular matrix (ECM) comprise a dynamic regulatory system responsible for tissue morphogenesis during development, as well as in response to injury [1,2]. However, much of the research in biomaterial development for regenerative medicine applications has employed either cell seeding atop 2-dimensional (2D) substrates that do not adequately recapitulate the 3D nature of native microenvironments, or spatially uniform and static materials that lack the heterogeneity that is found *in vivo*. As such, important causal relationships such as the dependence of stem cell morphology [3] and differentiation [4] on 2D substrate elasticity may not readily translate to 3D culture. Thus, the development of 3D hydrogel systems, particularly with spatially controlled features, would be an important advance for investigating basic questions in cell behavior and tissue development, as well as toward regenerative medicine applications.

While considerable progress has been made in developing uniform ECM-mimetic 3D scaffolds capable of promoting hydrogel remodeling [5,6] and even stem cell differentiation [7], one continuing challenge is the difficulty in translating patterning methods well established for 2D or laminated substrates to 3D to enable the necessary spatial control over materials. The patterning of 3D hydrogel systems has been limited to only a few techniques, and most of these rely on pre-fabrication before the introduction of cells due to cytocompatibility concerns [8,9]. Techniques have also been developed where cellular adhesion is patterned in 3D using click chemistry reactions [10] or through the introduction of a photodegradable linker [11] to alter cellular interactions to materials. These approaches use spatial control of adhesion to alter cellular behavior, but rely on complex chemistry and are only applicable to a few polymer systems.

To overcome these limitations, this report describes the development of a simple technique incorporating multiple modes of crosslinking, applied sequentially, to enable 3D spatially patterned remodeling of hydrogels. The technique is based on the basic understanding of how cells remodel certain crosslinks. These hydrogels support remodeling and infiltration of cells from *ex vivo* tissues (e.g., chick aortic arches) or by cells that are encapsulated directly in the hydrogels (e.g., human mesenchymal stem cells, hMSCs). Hyaluronic acid (HA) was used as the primary structural component in the current work due to its biocompatibility, hydrophilicity, importance *in vivo* [12,13], and past use in 3D hydrogel systems; [14–18] however, this approach can be easily applied to any polymeric material functionalized with compatible reactive groups.

---

* Corresponding author. Tel.: +1 215 898 8537; fax: +1 215 573 2071.
E-mail address: burdick2@seas.upenn.edu (J.A. Burdick).

0142-9612/$ – see front matter © 2010 Elsevier Ltd. All rights reserved.
doi:10.1016/j.biomaterials.2010.07.035

2. Materials and methods

All materials were purchased from Sigma–Aldrich unless otherwise stated.

2.1. AHA synthesis

Acrylated hyaluronic acid (AHA) was synthesized via a two-step protocol: (1) Synthesis of the tetrabutylammonium salt of HA (HA–TBA) was performed by reacting sodium hyaluronate (64 kDa, Lifecore) with the highly acidic ion exchange resin Dowex-100 and neutralization with 0.2M TBA-OH. (2) Coupling of acrylic acid (2.5 eq) and HA–TBA (1 eq, repeat unit) in the presence of dimethylamino pyridine (DMAP; 0.075 eq) and di-tert-butyl-dicarbonate (1.5 eq) in DMSO, followed by dialysis and lyophilization. Synthetic details (Fig. S1a), as well as the final structure and ^{1}H NMR spectrum of AHA (Fig. S1b) are provided in Supplementary Information.

2.2. Peptides

The cell adhesive oligopeptide GCGYG*RGDS*PG (MW: 1025.1 Da; italics indicate cell adhesive domain) and MMP-degradable oligopeptide GCRDGPQG↓IWGQDRCG (MW: 1754.0 Da; down arrow indicates site of proteolytic cleavage), both with >95% purity (per manufacturer HPLC analysis), were obtained from GenScript Corporation (Piscataway, NJ, USA).

2.3. Hydrogel formation

AHA was dissolved in sodium phosphate buffered saline (NaPBS buffer: 0.1 M sodium phosphate, 0.3 M total osmolarity, pH 8.0) containing Irgacure 2959 (I2959, Ciba) photoinitiator (final concentration of 0.05 wt%). I2959 was chosen due to its aqueous solubility and good cytocompatibility [19,20]. Sequentially crosslinked AHA hydrogels were synthesized using a two-step procedure of an addition reaction followed by radical polymerization. In the first step, stable "−UV" hydrogels were synthesized via addition reactions between AHA macromers (first reacted with the cell adhesive peptide to a final concentration of 2 mM at room temperature for 30 min) and MMP-degradable peptides (acrylates react with thiols from cysteines on peptides under these conditions) to consume 50% of the total available acrylate groups. Selected −UV gels were then exposed to 10 mW/cm^2 365 nm ultraviolet light (Omnicure S1000 UV Spot Cure System, Exfo, Ontario, Canada) for 4 min (secondary crosslinking) through glass coverslips to produce uniform "+UV" hydrogels. Spatial patterning of the hydrogels was possible by substituting 10k DPI photomasks (CAD/Art Services, Inc., Bandon, OR) for coverslips during the secondary step. For studies involving photopatterned gels, 5 nM methacrylated rhodamine (MeRho) was mixed into the prepolymer solution for visualization of +UV regions of the gels (methacrylates react extensively during the radical polymerization, but relative to acrylates, coupling is too slow during the addition reaction).

2.4. Microscopy

For all studies, confocal laser scanning microscopy (CLSM) images were obtained with a Zeiss LSM 510 Meta Confocal microscope (Carl Zeiss), using a DAPI/FITC/TRITC multi-track configuration at 5×, 10×, and 20× objectives. All CLSM images are projections of a 150 μm thick gel portion using a 15 μm slice thickness.

2.5. Hydrogel characterization

Samples were fabricated as described above and swelled to equilibrium in PBS for 24 h. Photopatterned acellular gels containing MeRho were imaged at the top and bottom surfaces, and the color intensity distribution versus horizontal distance was obtained using the "Plot Profile" tool in ImageJ (NIH). The elastic moduli of uniform and photopatterned AHA hydrogels were quantified using atomic force microscopy (AFM, Veeco Bioscope I). A silicon bead AFM tip with a spring constant of ~0.06 N m^{-1} was used to obtain force curves for individual points on the gel surface ($n = 10$ points chosen for each condition), from which a local elastic modulus was calculated. For photopatterned gels, points were chosen at random locations from the interior of −UV or +UV regions of the gel. To characterize the real-time change in hydrogel mechanical properties with crosslinking, the shear elastic modulus was measured via dynamic oscillatory shear rheometry at 1% strain and 1 Hz using an AR2000ex controlled stress rheometer (TA Instruments) with parallel plate geometry (20 mm diameter). Following the addition of crosslinker, the polymer solution was mixed and pipetted directly onto the bottom plate, and the top plate was lowered to contact the gelling solution with a 100 μm gap size. The evolution of the elastic stored modulus, G', and viscous loss modulus, G'', was monitored with time. The uniform −UV hydrogel was allowed to undergo addition crosslinking for 15 min to a peak value of ~0.8 kPa, at which point the gel was irradiated by 10 mW/cm^2 365 nm UV light (Omnicure S2000 Spot Curing System), resulting in a rapid increase in the elastic modulus to a peak value of ~5.1 kPa. The gel point (i.e., the intersection of G' and G'') occurred almost immediately after mixing of the two components (i.e., before the mixture was pipetted onto the rheometer stage) and thus does not appear on the displayed sweep.

To quantitatively assess degradation kinetics, uniform crosslinked −UV and +UV hydrogels were incubated in separate wells of a 24-well plate containing either 1.0 mL PBS or 1.0 mL PBS with 40 nM human MMP-2 (R&D Systems) on an orbital shaker at 37 °C. The solutions were refreshed every 48 h until complete degradation of −UV hydrogels occurred. The sample supernatants (frozen and stored at −20 °C after collection) were analyzed in triplicate via a modified uronic acid assay as previously reported [20]. For SEM analysis, uniform −/+ UV and 250 μm diameter dot photopatterned hydrogels were incubated with PBS containing MMP-2 as above until complete degradation of the uniform −UV hydrogels occurred. The samples were then flash frozen in liquid N$_2$, lyophilized, and imaged with a JEOL 7500 HR-SEM at 10 kV.

2.6. Chick aortic arch culture

Specific pathogen-free chick embryos (Charles River Labs) were sacrificed at day 14 after fertilization, and dissection and extraction of aortic arch samples (~1 mm^3 volume) were performed using aseptic techniques [21]. For encapsulation, arches were suspended in the precursor solution prior to the first crosslinking step. AHA hydrogels with encapsulated arches were incubated in basal medium with supplements (EGM-2 media; Lonza) with media replacement every 2–3 days. Following 3 weeks in culture, the gels were fixed with 10% formalin and stained with FITC-conjugated phalloidin using standard protocols.

2.7. hMSC cell culture

Human mesenchymal stem cells (hMSCs) were obtained from Lonza Corporation (Walkersville, MD). For encapsulation studies, hMSCs were expanded in growth media (α-MEM, 10% FBS, 1% L-Glutamine & penicillin–streptomycin) and encapsulated at passage 3 in AHA hydrogels at a density of 5×10^6 cells mL^{-1} by suspension in the precursor solution prior to the first crosslinking step. The constructs were maintained in 2 mL growth media (for remodeling studies, Fig. 5) or a mixed adipogenic/osteogenic inductive media (for differentiation studies, Fig. 6) in a 24-well plate and media was refreshed every 2–3 days until day 14. The adipogenic/osteogenic mixed media was made by combining commercially available osteogenic and adipogenic inductive media (R&D Systems) in a 1:1 ratio and supplementing with 1% (v/v) penicillin–streptomycin.

2.8. Live/dead staining

Following 14 days incubation in growth media, cell viability and morphology (for remodeling studies) were assessed using a live/dead staining kit (Molecular Probes).

2.9. Cellular aspect ratio measurements

Cellular aspect ratio is defined as the ratio of the maximum orthogonal length to width of each cell. To quantify, three random CLSM images of live/dead stained gels at 20× magnification were chosen from the interior of each gel; each image was used for ≥20 measurements of randomly selected cells, or $n \geq 60$ for each sample. The measured aspect ratios were then sorted into bins and reported as histograms.

2.10. Oil red O and ALP quantification

Following 14 days of incubation in mixed adipogenic/osteogenic inductive media, production of oil red O and ALP by hMSCs encapsulated within uniform −UV and +UV hydrogels was assessed quantitatively. For oil red O, hydrogels were stained with the marker as described in Supplementary Information (see Fig. S5 for representative stains). Quantification of the oil red O from the same samples was then performed as previously reported [22]. Briefly, oil red O was eluted from the stained hydrogels by incubation in 100% isopropanol for 30 min. Following manual digestion of the gels and centrifugation to remove cellular and gel debris, the supernatant absorbance containing the eluted oil red O was read at 500 nm. For ALP, hydrogels were manually digested in 250 μL CelLytic M cell lysis buffer, incubated at 45 °C for 1 h, and centrifuged to remove cellular debris. ALP production was then quantified by reacting 50 μL of the lysis buffer with an equal volume of substrate solution and measuring the absorbance at 405 nm. Quantitative values for oil red O and ALP were normalized to total dsDNA content, which was determined using the PicoGreen assay as previously reported [23].

2.11. Immunocytochemistry

Following 14 days incubation in mixed adipogenic/osteogenic inductive media, uniform −UV and +UV and photopatterned (250 μm stripes) hydrogels with encapsulated hMSCs were fixed overnight in 10% formalin. The gels were washed (PBS containing 0.1% Tween 20 and 3% bovine serum albumin), permeabilized with 0.25% Triton X-100, blocked with 10% goat serum in PBS, and incubated overnight at 4 °C with anti-human osteocalcin (1:10 dilution, mouse IgG) and anti-fatty acid binding protein (R&D Systems, 1:20 dilution, goat IgG) 1° Ab. Constructs were then washed and incubated for 2 h at room temperature with Alexa Fluor 488 anti-mouse (goat IgG) and Alexa Fluor 350 anti-goat (donkey IgG) 2° Ab for OC and FABP, respectively.

2.12. *Statistical analysis*

Values are reported as mean ± standard error of the mean (mechanics). Statistical differences between groups ($p < 0.05$) were determined using ANOVA in conjunction with Tukey's post hoc test (JMP software).

3. Results and discussion

A two-step protocol was used to synthesize sequentially crosslinked hydrogels. In the primary crosslinking step, a uniform (i.e., non-patterned) "−UV" hydrogel is formed using Michael-type reactivity between multi-acrylate HA macromers and bifunctional, proteolytically degradable peptides. Monofunctional, pendant RGDS-containing peptides are also added (prior to crosslinking) to incorporate cell adhesion. With these components (adhesion and proteolytic degradability), this hydrogel was expected to support cellular remodeling [5,24]. The primary addition step is performed in the presence of a photoinitiator (at this point, non-reactive) and designed so that only a portion of total available acrylate groups are consumed, making secondary free radical crosslinking possible. In the secondary step, −UV hydrogels are exposed to light to initiate free radical photopolymerization of the remaining acrylate groups. The resulting "+UV" hydrogels were expected to prevent remodeling due to the incorporation of non-degradable covalent crosslinks from kinetic chain formation. Since mesh sizes in the +UV hydrogels are orders of magnitude smaller than typical cell diameters [24,25], secondary crosslinking was also predicted to prevent cellular outgrowth from tissue and to confine encapsulated cells to a rounded morphology. This has been observed previously when cells are encapsulated in hydrogels using a purely radical polymerization [26–28].

With this technique, it is possible to synthesize and characterize hydrogels patterned with −UV (permissive) and +UV (inhibitory) regions (Fig. 1). Since the secondary crosslinking is initiated by light, spatially distinct zones of remodeling are created by applying a photomask to the gel surface prior to the secondary crosslinking (Fig. 1a). To assess pattern resolution with depth, methacrylated rhodamine (MeRho) was mixed into the prepolymer solution, which due to charge density and steric hindrance effects [29] only covalently incorporates into the network during the secondary radical crosslinking. The pattern fidelity at the top and bottom surfaces of a hydrogel photopatterned with 250 μm stripes was confirmed qualitatively by visualization using laser scanning confocal microscopy (LSCM) (Fig. 1a), and quantitatively by plotting the average color intensity versus horizontal distance across the pattern (Fig. 1b). These results demonstrate the retention of high resolution patterns throughout the hydrogel volume.

Mechanical testing of photopatterned hydrogels was then carried out to determine if differences in gel structure predictably instructs differences in mechanics of −UV and +UV environments. Atomic force microscopy (AFM) was used to characterize the local elastic modulus of −UV and +UV regions of photopatterned hydrogels and for uniform gels (Fig. 2a). As expected, the increased crosslink density as a result of photopolymerization led to an increase in mechanical properties from 6.3 ± 0.7 kPa to 18.0 ± 1.5 kPa in −UV and +UV uniform hydrogels, respectively, and from 6.3 ± 1.0 kPa to 15.2 ± 2.4 kPa in −UV and +UV regions of photopatterned gels, respectively. Further, the increase in elastic modulus as a result of secondary crosslinking was observed in rheometry studies, which showed a rapid increase in shear modulus with light exposure similar in fold to that observed with AFM testing (Fig. 2b). The mechanical properties in each environment can be tuned for individual applications by adjusting the macromer concentration and ratio of addition to radical crosslinking, both of which were kept constant (3 wt% and 1:1, respectively) in this study.

To demonstrate that the incorporation of non-degradable covalent kinetic chains restricts protease-mediated remodeling, we exposed hydrogels to exogenous MMP-2. When incubated in PBS containing 40 nM MMP-2, uniform −UV hydrogels underwent complete degradation (i.e., 100% uronic acid release) within 12 days, whereas very limited degradation (16.8 ± 2.1% uronic acid release) was observed with uniform +UV hydrogels (Fig. 3a). The small degree of mass loss in +UV hydrogels may be due to hydrolysis of ester linkages in the crosslinks or a soluble fraction after crosslinking. To assess the degradation of patterned hydrogels, both uniform −UV and +UV and patterned gels (250 μm dots) were incubated in 40 nM MMP-2 and imaged using scanning electron microscopy (SEM) (Fig. 3b). As expected, incubation with MMP-2 for 12 days led to complete degradation of −UV gels, but did not significantly affect the surface topography of +UV regions, whereas patterned gels degraded only in the −UV regions of the gel (i.e., the

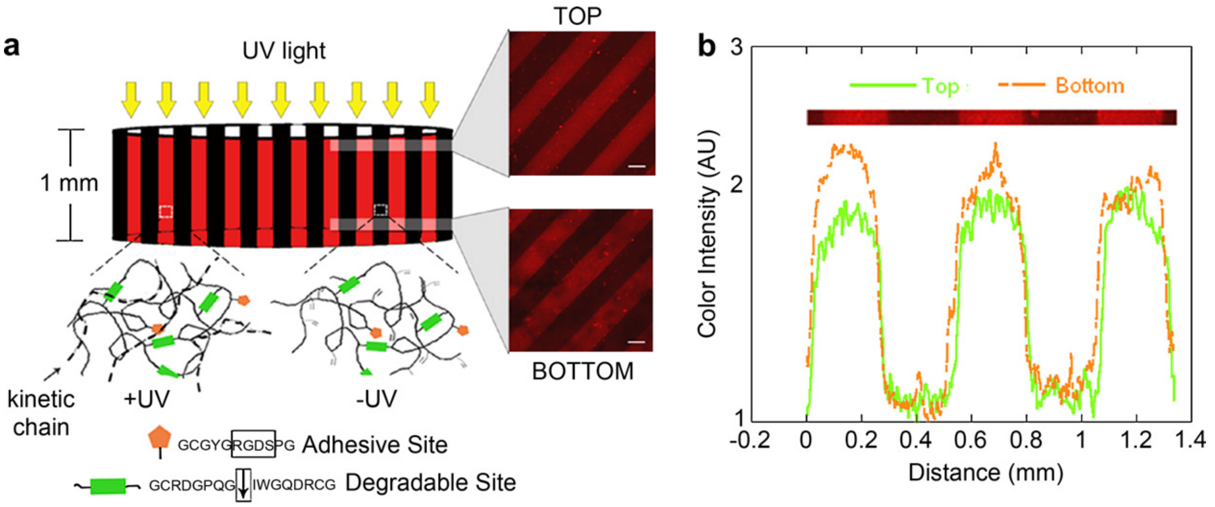

Fig. 1. Photopatterning of AHA hydrogels. **(a)** Schematic of a sequentially crosslinked hydrogel photopatterned using a high resolution photomask. Laser scanning confocal microscopy (LSCM) images are shown from the top and bottom surfaces of a hydrogel photopatterned with 250 μm stripes. Light-initiated radical polymerization and kinetic chain formation only occurs in exposed (+UV) regions, whereas the unexposed (−UV) regions only consist of peptide crosslinks, resulting in spatially precise zones of crosslink type as illustrated schematically below the gel diagram. Scale bars = 200 μm. **(b)** Quantification of photopattern fidelity at the top and bottom gel surfaces from images in **(a)** scanned perpendicularly with respect to the pattern.

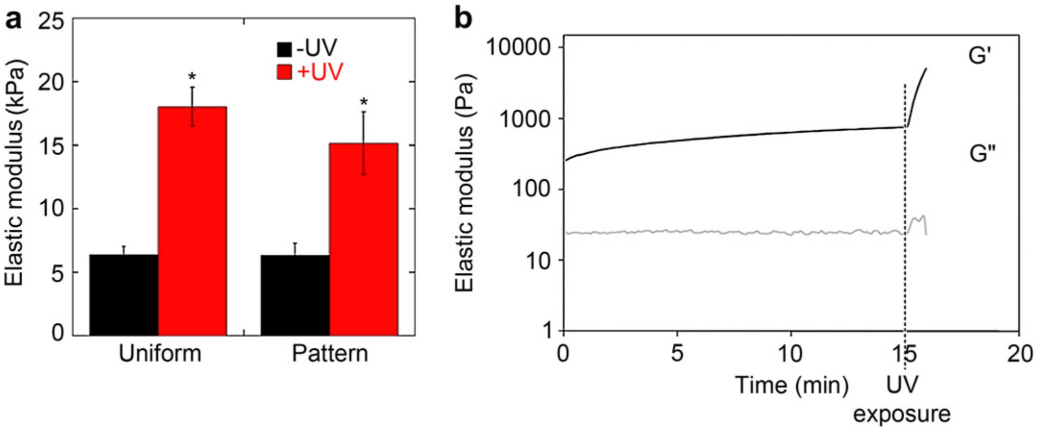

Fig. 2. Mechanical properties of photopatterned and uniform AHA hydrogels. **(a)** Elastic modulus of uniform −UV and +UV hydrogels, and −UV and +UV regions of photopatterned hydrogels measured by atomic force microscopy. * Denotes statistically significant difference ($p < 0.05$) between +UV and −UV conditions for uniform and patterned gels. **(b)** The storage (G′) and loss (G″) moduli of a uniform sequentially crosslinked AHA gel measured by parallel plate oscillatory shear rheometry, with secondary crosslinking performed after 15 min of primary crosslinking.

circular dot). Patterned degradation of the gels was further confirmed by reacting macromers with thiolated FITC prior to crosslinking and observing the progressive loss of fluorescence within −UV regions upon incubation with MMP-2 (Fig. S2). These results support the hypothesis that the incorporation of non-degradable covalent kinetic chains from secondary crosslinking restricts the protease-mediated remodeling observed in −UV environments of uniform and patterned gels. Additionally, the degradation behavior further illustrates the potential tunability afforded by these techniques, as the rate of remodeling can be matched to tissue engineering applications of interest by varying both the total crosslink concentration and the ratio of degradable to non-degradable crosslinks.

To assess whether the degradation behavior of the gels translates to directed cellular behavior, ~1 mm^3 chick aortic arch samples or hMSCs were mixed with MeRho into the macromer solution and encapsulated in both uniform and photopatterned gels. Aortic arches are useful as a model system for tissue growth, since outgrowth can be readily imaged and quantified [21]. As illustrated in Fig. 4, the degree of cellular outgrowth from aortic arch samples was dependent on the hydrogel composition. Arches encapsulated in uniform −UV hydrogels exhibited robust isotropic radial outgrowth (0.92 mm ± 0.18 mm) compared to largely restricted outgrowth in uniform +UV samples (0.14 mm ± 0.02 mm) (Fig. 4a). When arch samples were encapsulated in gels synthesized with various patterns of light exposure and visualized using confocal microscopy (Fig. 4b), outgrowth as a result of gel remodeling was only observed into biodegradable −UV (i.e., black) versus restrictive +UV (i.e., red from MeRho incorporation) regions of the gel. The representative x–y and z coordinate projections shown are from a focal region (150 µm thickness) of the gel ~500 µm above the arch sample, highlighting the capacity of the patterned gel structures to direct cell migration over a length-scale comparable to the sample thickness (~1 mm).

The responses of encapsulated hMSCs to each hydrogel composition (Fig. 5) corroborated the arch findings and provide further evidence of control of cellular remodeling using sequential crosslinking. As shown in representative CLSM projections from the interior of the gels (Fig. 5a), cells encapsulated in uniform −UV hydrogels for 14 days locally degraded the matrix, spread and exhibited high aspect ratios (i.e., the ratio of the longest dimension of the cell to the shortest orthogonal dimension) (Fig. 5b). We and others have shown previously [5,30] that the inclusion of both sites for proteolytic degradation and for adhesion (e.g., RGD) is necessary

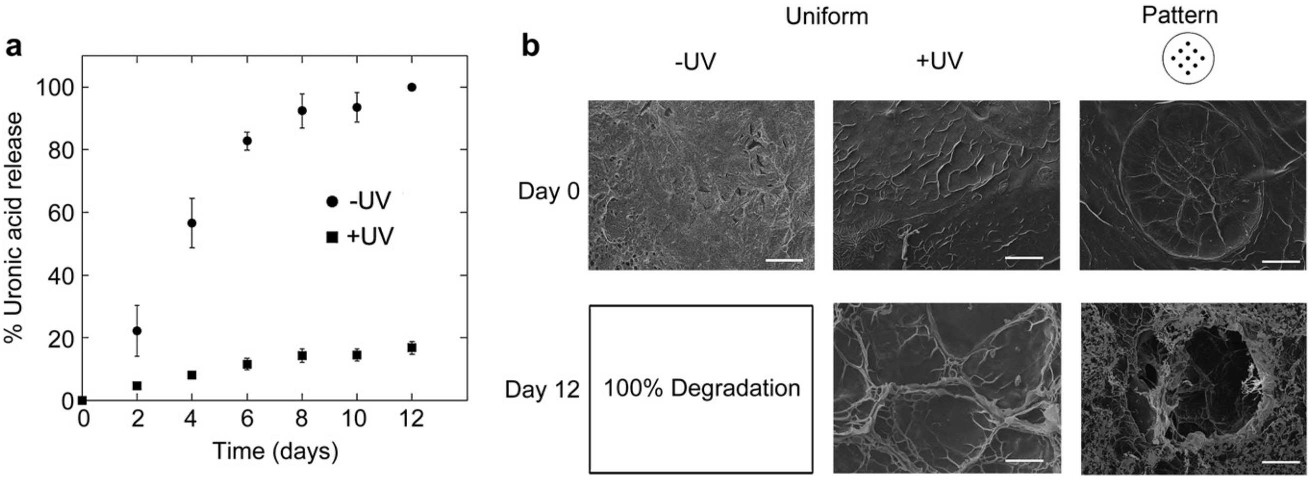

Fig. 3. Enzymatic degradation of sequentially crosslinked AHA hydrogels by exogenous MMP-2. **(a)** Degradation kinetics of uniform −UV or +UV AHA hydrogels (50% theoretical consumption of acrylates during primary addition crosslinking) in the presence of 40 nM MMP-2. **(b)** Representative scanning electron microscopy (SEM) images of either uniform −UV or +UV hydrogels or hydrogels photopatterned using 250 µm diameter black dots at day 0 (i.e., no degradation) and 12 (following complete degradation of uniform −UV hydrogels) of incubation with 40 nM MMP-2. Scale bars = 100 µm.

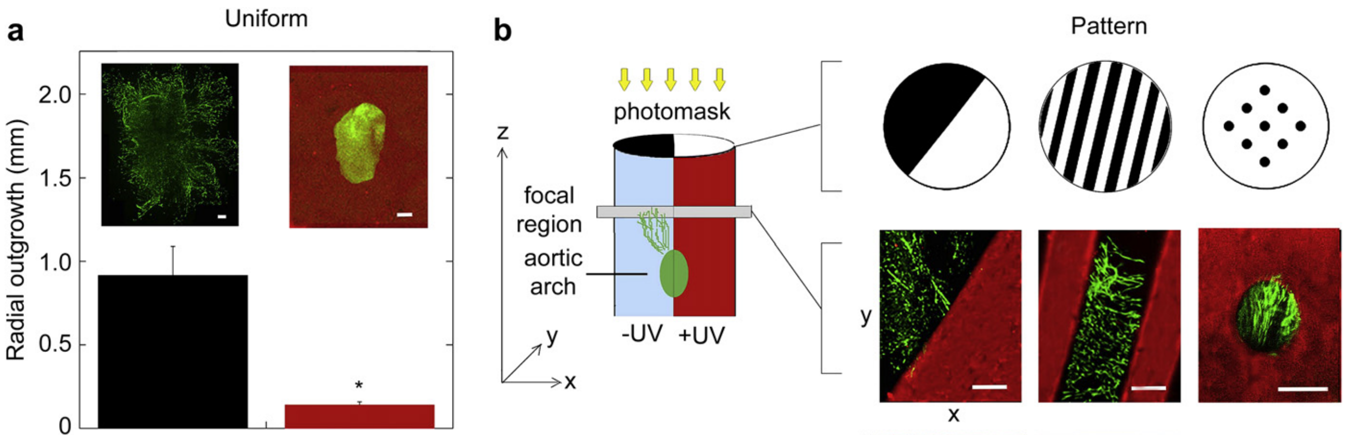

Fig. 4. Chick aortic arch sprouting within AHA hydrogels. **(a)** Actin (FITC-phalloidin) staining of outgrowth within uniform −UV and +UV hydrogels. Representative LSCM images (5× magnification) are shown from the plane of isotropic radial (i.e., in the x–y plane) outgrowth into the samples and used for quantification ($n \geq 10$ measurements/sample, $n = 3$ samples/condition). * Denotes statistically significant difference between uniform −UV and +UV conditions ($p < 0.01$). Scale bars = 200 μm. **(b)** Representative LSCM images (10× magnification) of photopatterned AHA hydrogels at a focal plane ~500 μm above the arch samples. Cellular outgrowth from the arch samples (shown by staining for actin) is limited to permissive −UV regions of the hydrogels. Below each pattern schematic are the corresponding x–y and z coordinate scans. Scale bars = 200 μm.

to support cellular spreading, and that the use of alternate crosslinkers (e.g., dithiothreitol or scrambled sequences) and/or the lack of adhesion sites restrict cells to a rounded morphology. Cells encapsulated in uniform +UV gels, in contrast to −UV gels, remained completely rounded, with almost all cells exhibiting an aspect ratio between 1 and 2. Cells in both conditions exhibited good viability (~85% and 83% in −UV and +UV uniform gels, respectively) with no significant difference between conditions, as quantified from live/dead staining (Fig. S3). Photopatterning of hydrogels resulted in −UV and +UV zones that recapitulated the behavior observed in the corresponding uniform hydrogels with single cell resolution. This is illustrated qualitatively, in the CLSM projections, and quantitatively, in the good agreement of the aspect ratio distributions with the respective uniform compositions. Taken together, the responses of cells from tissue (aortic arches) and in suspension (hMSCs) demonstrates that secondary crosslinking, applied to −UV gels uniformly or with patterning through masks, switches AHA hydrogels from a "permissive" to "inhibitory" state with respect to remodeling, outgrowth, and spreading.

Scaffold remodeling is a critical parameter in biomaterial systems, since differences in the degradability of hydrogel microenvironments lead to differences in temporal cell adhesivity and spreading, established inputs to hMSC differentiation [31,32]. Recent reports [33,34] using a mixed adipogenic/osteogenic inductive medium demonstrated a direct dependence of differentiation on morphology-mediated cytoskeletal tension. When cultured on 2D substrates, spread cells with spindle-like morphologies differentiated down a cytoskeleton-rich osteogenic lineage, whereas cytoskeleton-poor rounded cells followed an adipogenic fate. Follow-up studies indicated that these fate decisions may be due to a tension-mediated switch involving the Rho and ROCK signalling pathways [35]. However, the precise effect of spreading on stem cell fate has not been replicated in 3D hydrogel systems, possibly due to limitations in previous material systems. We hypothesized that spatially defined differences in hydrogel remodeling and subsequent tension-mediated cell spreading could induce a similar switch in hMSC differentiation in uniform and patterned hydrogels. Specifically, spread and rounded hMSCs in

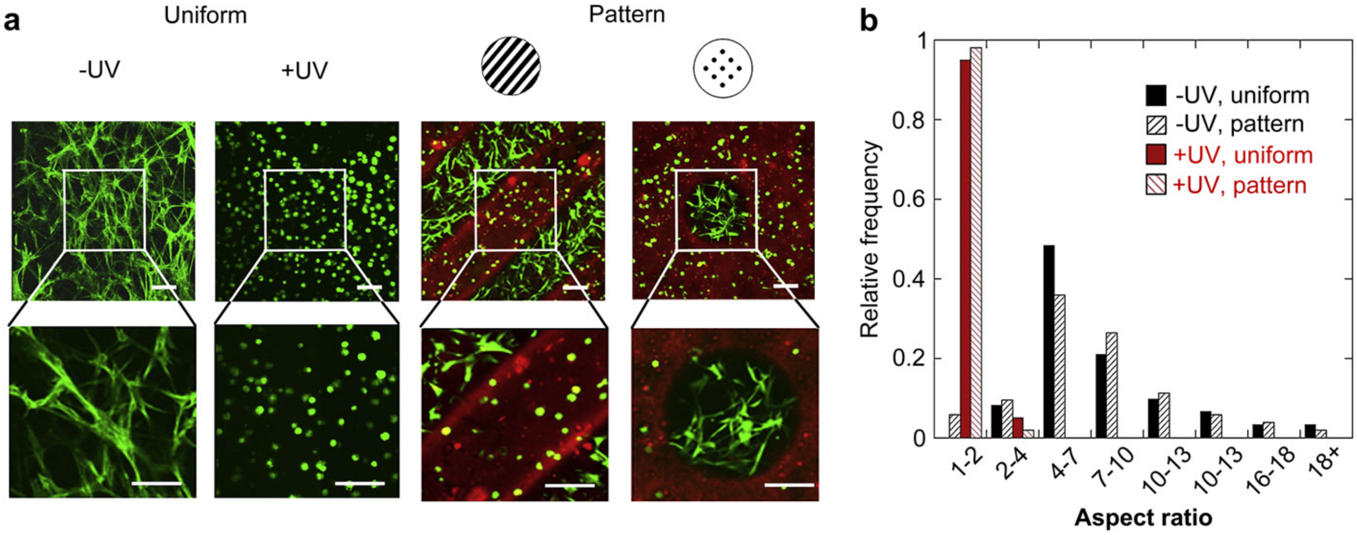

Fig. 5. Hydrogel remodeling by encapsulated hMSCs. **(a)** Images of encapsulated hMSCs (stained with calcein) in uniform and photopatterned AHA hydrogels. Spreading only occurs in the permissive −UV regions. Scale bars = 100 μm. **(b)** Histograms of the cellular aspect ratio (the ratio of the longest ratio to shortest dimension of encapsulated cells) for these same groups. All cultures were for 14 days.

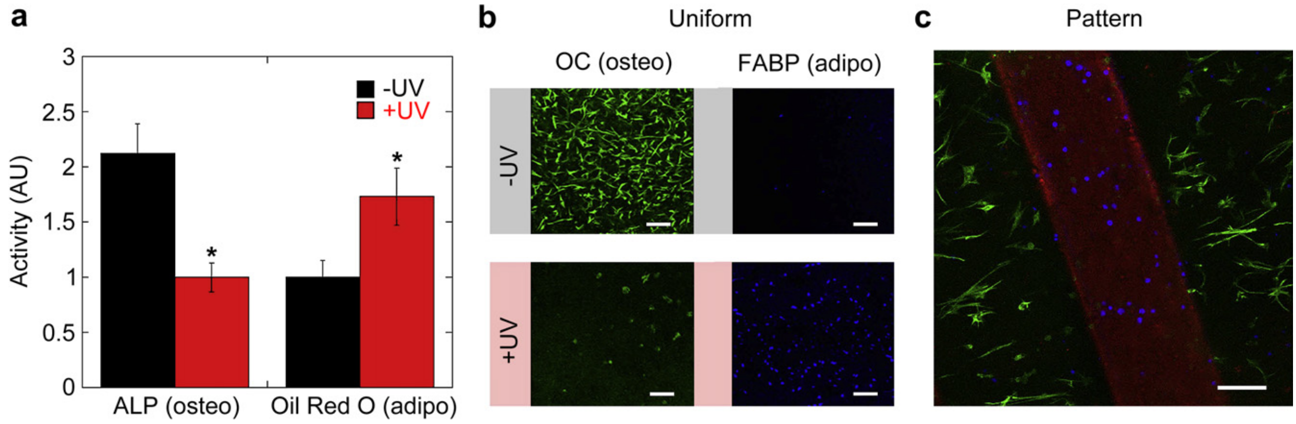

Fig. 6. Spatially patterned hMSC lineage commitment in mixed adipogenic/osteogenic culture media. **(a)** Quantitative assays for markers of osteogenic (alkaline phosphatase) and adipogenic (oil red O) hMSC differentiation following 14 days of mixed media culture within uniform −UV and +UV hydrogels. * Denotes statistically significant differences ($p < 0.05$) between conditions. **(b)** Representative immunostaining images for fatty acid binding protein (blue; adipogenesis) and osteocalcin (green; osteogenesis) from the interior of uniform −UV and +UV hydrogels, with channels shown separately for ease of viewing. Scale bars = 100 μm. **(c)** Representative immunostaining images for the same targets from the interior of a hydrogel photopatterned with 250 μm stripes. Scale bar = 100 μm.

permissive −UV and inhibitory +UV environments were expected to undergo primarily osteogenesis and adipogenesis, respectively, based simply on morphology. To test this hypothesis, low passage hMSCs were encapsulated in uniform −UV and +UV hydrogels and hydrogels photopatterned with a 250 μm stripe pattern. 14 days following incubation in 1:1 adipogenic/osteogenic media, hMSC differentiation was assessed by quantitative protein assays for markers of osteogenesis (alkaline phosphatase, ALP) and adipogenesis (oil red O), gene expression analysis, histological staining for ALP and oil red O, and immunostaining for osteocalcin (OC; osteogenic differentiation) and fatty acid binding protein (FABP; adipogenic differentiation). Our choice of differentiation markers was based on literature demonstrating specificity of each marker to its respective lineage at 14 days following hMSC induction [36,37].

Consistent with our hypothesis and in good agreement with the described previous reports, Fig. 6 illustrates a clear dependence of hMSC differentiation within the respective AHA hydrogel microenvironments on cell morphology. Results of quantitative assays for ALP and oil red O in normalized arbitrary units of activity are shown in Fig. 6a. ALP activity (osteogenic marker) in uniform −UV hydrogels (where cell spreading is permitted) was 2.1 ± 0.3, compared to 1.0 ± 0.1 within +UV gels (where cell spreading is restricted). In contrast, oil red O activity (adipogenic marker) was 1.7 ± 0.3 in uniform +UV hydrogels compared to 1.0 ± 0.2 within −UV gels. Representative x–y coordinate projections from the interior of uniform −UV and +UV gels stained for OC (osteogenic marker) and FABP (adipogenic marker) are shown in Fig. 6b. Cells encapsulated in −UV gels underwent primarily osteogenic differentiation, as illustrated by dense staining of OC in spindle-shaped cells, compared to sparse staining of comparatively rounded cells in the +UV constructs. The opposite trend was observed for expression of FABP; rounded cells in +UV stained predominantly for this adipogenic marker relative to cells in −UV gels. Lineage specification of hMSCs in uniform −UV and +UV environments was further confirmed via quantitative PCR and cytochemical staining (Fig. S4–S5). In photopatterned AHA hydrogels, multi-lineage hMSC differentiation based on the local gel structure was confirmed by immunostaining for the same targets (Fig. 6c). Cells in −UV and +UV regions were induced primarily down the osteogenic and adipogenic lineages, respectively.

Interestingly, the observed differentiation switch occurred despite a mismatch in the mechanical properties traditionally associated with each lineage [4,38,39] (i.e., hMSCs in the higher elastic modulus +UV environment were induced toward an adipogenic, not osteogenic fate). Our results contrast, for example, those of a recent report by Heubsch et al. [39] describing the dependence of MSC differentiation on the elastic modulus of physically crosslinked 3D alginate scaffolds with a constant adhesive ligand concentration. In these studies, encapsulated hMSCs differentiated based on the gel elastic modulus (2.5–5 kPa and 11–30 kPa for adipogenesis and osteogenesis, respectively); however, the cells maintained a grossly rounded morphology in all conditions. The authors provide evidence that lineage commitment was based on the ability of the cells to reach through the surrounding mesh and utilize traction forces to reorganize and cluster adhesive ligands. The degree of cytoskeletal tension and adhesion ligand clustering was shown to correlate directly with the gel modulus, providing a mechanistic basis for osteogenic versus adipogenic differentiation in the stiffer versus more compliant gels.

In our work, we hypothesize that kinetic chain formation in the +UV hydrogel environments, despite causing an increase in mechanical properties to a more typical osteogenic range (~15–18 kPa), functions as a non-degradable steric barrier, blocking the ability of encapsulated hMSCs to spread. In contrast, spread hMSCs in permissive −UV hydrogels undergo osteogenesis, potentially since their ability to spread allows them to apply greater tensions on the matrix, despite initial mechanical properties (~6 kPa) that are lower than the +UV system that supported adipogenesis. These differences illustrate that, relative to 2D systems, 3D substrate properties including elastic modulus, adhesive ligand density, degradability and crosslink type may act collectively on encapsulated cell fate, a dynamic process that is less amenable to generalized trends based upon any single property.

4. Conclusions

The sequential crosslinking and photopatterning techniques presented here constitute a simple but powerful technique to control hydrogel remodeling in 3D. The choice of material properties (e.g., choice of polymer, type of functionalization, modification efficiency) and experimental parameters (e.g., macromer weight percentage and ratio of crosslinking types) are among the design parameters kept constant in the current work that can be adjusted to tune degradation and remodeling rates for individual applications. The use of a light-initiated secondary crosslinking step may also enable more advanced processing capabilities, such as the synthesis of a hydrogel with a gradient of crosslink type ratio (i.e., by using a syringe pump to translate a photomask laterally above the gel during light exposure). Such techniques may be valuable for other basic cell-material interaction studies or advanced tissue engineering applications, including the engineering *in vitro* of clinically relevant tissues with interfaces (e.g., osteochondral defects) or anisotropic properties (e.g., vascular or nervous tissues). Importantly, this technology is applicable to a range of currently used polymeric biomaterials and incorporates spatial control that is crucial in developing complex microenvironments.

Acknowledgements

This work was supported by funding from a Fellowship in Science and Engineering from the David and Lucile Packard Foundation (JAB) and a CAREER award (JAB) and Graduate Research Fellowship (SK) from the National Science Foundation. The authors would like to thank the following individuals for helpful discussions and experimental assistance: R. Marklein, J. Ifkovits, V. Ramanan, J. Katz, Dr. M. Charati, Dr. C. Shen and Dr. J. Miller.

Appendix. Supplementary information

Supplementary information associated with this article can be found in the on-line version, at doi:10.1016/j.biomaterials.2010.07.035.

Appendix

Figures with essential color discrimination. Figs. 1, 2, 4–6 in this article are difficult to interpret in black and white. The full color images can be found in the on-line version, at doi:10.1016/j.biomaterials.2010.07.035.

References

[1] Hynes R. Integrins: bidirectional, allosteric signalling machines. Cell 2002;110(6):673–87.
[2] Geiger B, Bershadsky A. Exploring the neighborhood: adhesion-coupled cell mechanosensors. Cell 2002;110(2):139–42.
[3] Marklein R, Burdick J. Spatially controlled hydrogel mechanics to modulate stem cell interactions. Soft Matter 2010;6(1):136–43.
[4] Engler A, Sen S, Sweeney H, Discher D. Matrix elasticity directs stem cell lineage specification. Cell 2006;126(4):677–89.
[5] Lutolf M, Raeber G, Zisch A, Tirelli N, Hubbell J. Cell-responsive synthetic hydrogels. Adv Mater 2003;15(11):888–92.
[6] Kim J, Kim I, Cho T, Lee K, Hwang S, Tae G, et al. Bone regeneration using hyaluronic acid-based hydrogel with bone morphogenic protein-2 and human mesenchymal stem cells. Biomaterials 2007;28(10):1830–7.
[7] Benoit D, Schwartz M, Durney A, Anseth K. Small functional groups for controlled differentiation of hydrogel-encapsulated human mesenchymal stem cells. Nat Mater 2008;7(10):816–23.
[8] Lee S, Moon J, West J. Three-dimensional micropatterning of bioactive hydrogels via two-photon laser scanning photolithography for guided 3D cell migration. Biomaterials 2008;29(20):2962–8.
[9] Musoke-Zawedde P, Shoichet M. Anisotropic three-dimensional peptide channels guide neurite outgrowth within a biodegradable hydrogel matrix. Biomed Mater 2006;1(3):162–9.
[10] DeForest C, Polizzotti B, Anseth K. Sequential click reactions for synthesizing and patterning three-dimensional cell microenvironments. Nat Mater 2009;8(8):659–64.
[11] Kloxin A, Kasko A, Salinas C, Anseth K. Photodegradable hydrogels for dynamic tuning of physical and chemical properties. Science 2009;324(5923):59–63.
[12] Yung S, Thomas G, Davies M. Induction of hyaluronan metabolism after mechanical injury of human peritoneal mesothelial cells in vitro. Kidney Int 2000;58(5):1953–62.
[13] Jiang D, Liang J, Noble P. Hyaluronan in tissue injury and repair. Annu Rev Cell Dev Biol 2007;23:435–61.
[14] Leach J, Bivens K, Collins C, Schmidt C. Development of photocrosslinkable hyaluronic acid-polyethylene glycol-peptide composite hydrogels for soft tissue engineering. J Biomed Mater Res A 2004;70(1):74–82.
[15] Chung C, Burdick J. Influence of three-dimensional hyaluronic acid microenvironments on mesenchymal stem cell chondrogenesis. Tissue Eng Part A 2009;15(2):243–54.
[16] Sakai Y, Matsuyama Y, Takahashi K, Sato T, Hattori T, Nakashima S, et al. New artificial nerve conduits made with photocrosslinked hyaluronic acid for peripheral nerve regeneration. Biomed Mater Eng 2007;17(3):191–7.
[17] Sahoo S, Chung C, Khetan S, Burdick J. Hydrolytically degradable hyaluronic acid hydrogels with controlled temporal structures. Biomacromolecules 2008;9(4):1088–92.
[18] Ji Y, Ghosh K, Shu X, Li B, Sokolov J, Prestwich G, et al. Electrospun three-dimensional hyaluronic acid nanofibrous scaffolds. Biomaterials 2006;27(20):3782–92.
[19] Williams C, Malik A, Kim T, Manson P, Elisseeff J. Variable cytocompatibility of six cell lines with photoinitiators used for polymerizing hydrogels and cell encapsulation. Biomaterials 2005;26(11):1211–8.
[20] Burdick J, Chung C, Jia X, Randolph M, Langer R. Controlled degradation and mechanical behavior of photopolymerized hyaluronic acid networks. Biomacromolecules 2005;6(1):386–91.
[21] Miller J, Shen C, Legant W, Baranski J, Blakely B, Chen C. Bioactive hydrogels made from step-growth derived PEG-peptide macromers. Biomaterials 2010;31(13):3736–43.
[22] Mauney J, Volloch V, Kaplan D. Matrix-mediated retention of adipogenic differentiation potential by human adult bone marrow-derived mesenchymal stem cells during ex vivo expansion. Biomaterials 2005;26(31):6167–75.
[23] Singer V, Jones L, Yue S, Haugland R. Characterization of PicoGreen reagent and development of a fluorescence-based solution assay for double-stranded DNA quantitation. Anal Biochem 1997;249(2):228–38.
[24] Kim J, Park Y, Tae G, Lee K, Hwang S, Kim I, et al. Synthesis and characterization of matrix metalloprotease sensitive-low molecular weight hyaluronic acid based hydrogels. J Mater Sci Mater Med 2008;19(11):3311–8.
[25] Chung C, Mesa J, Miller G, Randolph M, Gill T, Burdick J. Effects of auricular chondrocyte expansion on neocartilage formation in photocrosslinkable hyaluronic acid networks. Tissue Eng 2006;12:2665–73.
[26] Chung C, Erickson I, Mauck R, Burdick J. Differential behavior of auricular and articular chondrocytes in hyaluronic acid hydrogels. Tissue Eng Part A 2008;14(7):1121–31.
[27] Burdick J, Anseth K. Photoencapsulation of osteoblasts in injectable RGD-modified PEG hydrogels for bone tissue engineering. Biomaterials 2002;23(22):4315–23.
[28] Lee H, Lee J, Chansakui T, Yu C, Elisseeff J, Yu S. Collagen mimetic peptide-conjugated photopolymerizable PEG hydrogel. Biomaterials 2006;27(30):5268–76.
[29] Osman R, Namboodiri K, Weinstein H, Rabinowitz J. Reactivities of acrylic and methacrylic acids in a nucleophilic addition model of their biological activity. J Am Chem Soc 1988;110(6):1701–7.
[30] Khetan S, Katz J, Burdick J. Sequential crosslinking to control cellular spreading in 3-dimensional hydrogels. Soft Matter 2009;5:1601–6.
[31] Senechal H, Wahrmann J, Delain D, Macieira-Coelho A. Modulation of differentiation in vitro. II. Influence of cell spreading and surface events on myogenesis. In Vitro 1984;20(9):692–8.
[32] Scintu F, Reali C, Pillai R, Badiali M, Sanna M, Argiolu F, et al. Differentiation of human bone marrow stem cells into cells with a neural phenotype: diverse effects of two specific treatments. BMC Neurosci 2006;7:14.
[33] Kilian K, Bugarija B, Lahn B, Mrksich M. Geometric cues for directing the differentiation of mesenchymal stem cells. Proc Natl Acad Sci U S A 2010;107(11):4872–7.
[34] Ruiz S, Chen C. Emergence of patterned stem cell differentiation within multicellular structures. Stem Cells 2008;26(11):2921–7.
[35] McBeath R, Pirone D, Nelson C, Bhadriraju K, Chen C. Cell shape, cytoskeletal tension, and RhoA regulate stem cell lineage commitment. Dev Cell 2004;6(4):483–95.
[36] Caballero M, Reed C, Madan G, Van Aalst J. Osteoinduction in umbilical cord- and palate periosteum-derived mesenchymal stem cells. Ann Plast Surg 2010;64(5):605–9.
[37] Podechard N, Fardel O, Corolleur M, Bernard M, Lecureur V. Inhibition of human mesenchymal stem cell-derived adipogenesis by the environmental contaminant benzo(a)pyrene. Toxicol In Vitro 2009;23(6):1139–44.
[38] Pek Y, Wan A, Ying J. The effect of matrix stiffness on mesenchymal stem cell differentiation in a 3D thioxtropic gel. Biomaterials 2010;31:385–91.
[39] Huebsch N, Arany P, Mao A, Shvartsman D, Ali O, Bencherif S, et al. Harnessing traction-mediated manipulation of the cell/matrix interface to control stem-cell fate. Nat Mater 2010;9:518–26.